PERGAMON

AE International – North America

Atmospheric Environment 37 (2003) 789–802

ATMOSPHERIC ENVIRONMENT

www.elsevier.com/locate/atmosenv

Airborne measurements of aerosol extinction in the lower and middle troposphere over Wyoming, USA

Ziguang Han, Derek C. Montague*, Jefferson R. Snider

Department of Atmospheric Science, University of Wyoming, Laramie, WY 82071-3038, USA

Received 9 April 2002; accepted 7 November 2002

Abstract

Particle size distributions, and scattering and absorption coefficients were measured over the Green River basin of Wyoming during the Southwest Wyoming Visibility Study (SWYVIS) in February and March 1996. Eleven flights were carried out, using the Wyoming King Air research aircraft. In the least polluted regions of the planetary boundary layer, particle number densities detected in the diameter range 0.13–3.0 μm were $<100\,cm^{-3}$. Aloft, in the stable air of the free troposphere, they were generally even lower, often falling to a few tens of particles per cm^3. Analyses of bulk aerosol filter samples showed that organic carbonaceous material was the dominant chemical component, with sulfate and refractory species being the largest inorganic components. Combining the filter data with separately measured black carbon mass loading values allowed refractive indices for the aerosol to be calculated, so that PCASP measured size distributions could be revised. Characterizing size parameters were obtained by fitting particle populations to bimodal lognormal distributions. Particle size distributions were somewhat broader at higher altitudes so that larger particles made greater contributions to extinction. Optical closure was attempted by comparing scattering and total extinctions computed by Mie theory with the corresponding values derived from the observations. While the calculated and measured single scattering albedo average values were in reasonably good agreement, even though individual pairs of values sometimes differed significantly, computed scattering coefficients often exceeded those derived from the measurements, by an average of 60%. Reasons for this discrepancy are explored, including the possible modification of the size distribution by partial or total volatilization of particles within the nephelometer and its inlet.

Keywords: Scattering extinction; Absorption extinction; Optical closure; Vertical profile; Aircraft sampling

1. Introduction

The growing awareness of the extent of aerosol involvement in a wide range of atmospheric phenomena from air pollution, with its attendant health and aesthetic impacts, to global climate change and ozone depletion issues, has stimulated an increasing number of observational studies of aerosol physical and chemical properties. Despite these efforts, accurate quantification of how aerosols directly and indirectly affect atmospheric radiative properties through their scattering and absorption interactions with both solar and terrestrial radiation, and their impact on cloud formation processes, remains elusive. Understanding the potential for future climate change primarily motivates most current studies. Of secondary interest are visibility issues, of both practical and aesthetic concern. Resolution of the outstanding questions is complicated by the time-dependent heterogeneous nature of the aerosol distribution, in terms of concentration, composition, and particle size. Surface studies capture temporal but not spatial variability, in contrast to those derived from remotely sensed radiance measurements of satellite-mounted instruments such as AVHRR (Husar et al.,

*Corresponding author. Tel.: +1-307-766-4949; fax: +1-307-766-2635.

E-mail address: montague@uwyo.edu (D.C. Montague).

1352-2310/03/$ - see front matter © 2002 Elsevier Science Ltd. All rights reserved.
doi:10.1016/S1352-2310(02)00952-4

1997), which encompass both. However, while satellite instruments offer the advantage of extended coverage in time and space, calibration of the retrieval products is still necessary and ideally requires three-dimensional in situ measurements for appropriate comparisons.

Aircraft observations afford the principal advantage of yielding detailed information on aerosol properties with height, albeit within short time periods over geographic areas of limited extent, thereby enabling the question of inhomogeneities of aerosol properties in the vertical to be addressed (Kim et al., 1993a; Pinnick et al., 1993; Raga and Jonas, 1995; Clarke et al., 1996; Sheridan and Ogren, 1999). Airborne observations that are sufficiently comprehensive to inter-relate the optical, physical, and chemical properties of particulates have been carried out relatively infrequently. Examples in the marine environment include NARE-96 (Cowling et al., 1998), ACE-1 (Bates et al., 1998), ACE-2 (Collins et al., 2000a; Öström and Noone, 2000), and INDOEX (de Reuss et al., 2001). Over coastal and continental locations, following earlier work of Rosen et al. (1992), Kim et al. (1993a), Gunter et al. (1993), Pinnick et al. (1993) and Gunter (1994), more elaborate airborne data sets have been acquired in the Arctic (Hegg et al., 1996), in the US mid-Atlantic coastal region (Hegg et al., 1997; Hartley et al., 2000), and over the Los Angeles Basin (Collins et al., 2000b), among others.

Few airborne studies have been carried out over remote continental locations, where aerosol mass loadings are frequently low and anthropogenic influences minimal. Observations from such regions are important to establish baseline comparison data sets, despite the inherent difficulties in obtaining the measurements. For example, low particulate mass loadings make comprehensive measurements of aerosol composition especially challenging from airborne platforms, particularly if time-dependent size-resolved composition is desired. Furthermore, the aerosol can be chemically and morphologically more complex over land, thereby complicating attempts to relate aerosol optical properties to physical and chemical characteristics.

While pristine air quality unaffected by human activities is no longer found within the continental USA or other populated continental areas, anthropogenic impacts are minimized in much of Wyoming. Data from the Bridger Wilderness Area (WY) Interagency Monitoring of Protected Visual Environments (IMPROVE) monitor regularly show that site to be one of the least polluted in the contiguous USA, in terms of particulate mass loading and ozone levels, reflecting the absence of significant air pollutant sources in the region upwind (Malm et al., 2000). Similarly, the low particulate loading results in the visual range in Wyoming being frequently greater than in many other parts of the nation (Malm et al., 2000).

In this paper we report airborne observations of the atmospheric aerosol over southwest Wyoming, obtained during the Southwest Wyoming Visibility Study (SWYVIS) in February and March 1996. The broad objectives of SWYVIS were to characterize the air chemistry, air quality, and associated visibility parameters in the study region. By measuring the aerosol size distribution, chemical composition, and optical properties, a closure experiment (see, e.g. Quinn et al., 1995; Quinn and Coffman, 1998; Ross et al., 1998; Collins et al., 2000a, b; Philippin et al., 1998; Peseva et al., 2001) that compares computed aerosol optical properties with those observed, was carried out, for both clean and polluted air within the planetary boundary layer (PBL) and free troposphere aloft. Vertical profiles of aerosol size distribution, and observed and predicted scattering extinction are also reported.

2. The aircraft and its instrumentation

Observations were carried out during SWYVIS using the Wyoming King Air research aircraft, equipped with both a standard suite of meteorological and navigational instrumentation and a variety of aerosol and air chemistry monitors. Signals from the aerosol and air chemistry instrumentation were recorded by the on-board data acquisition system. Archived 1 Hz data values were used to derive time and height averages.

Aerosol particle scattering and absorption coefficients were measured with a Radiance Research M903 integrating nephelometer, calibrated prior to each flight using $CHClF_2$ (CFC22), and a Magee Scientific aethalometer (Hansen et al., 1984), respectively. Light attenuation by absorption was attributed entirely to black carbon (BC) (Gundel et al., 1984; Wolff, 1984).

Aerosol particle size distributions and were determined by a wing-tip pod mounted passive cavity aerosol spectrometer probe (PCASP-100X) (Particle Measuring Systems, Boulder, CO), which sizes particles in the nominal diameter (D) range from 0.13 to 3.0 μm in 15 channels. Calibration of the instrument was performed prior to the field campaign by the Atmospheric Environment Service of Canada (Liu et al., 1992). Sample heating in the PCASP as a result of both ram-heating from flow deceleration and mixing of the sample air with warmer sheath air is estimated to be 5°C. For typical SWYVIS ambient conditions (surface temperature range: −10°C to 10°C; relative humidity range: 15–75%) this heating would reduce the sampled air relative humidity (RH) to $35 \pm 30\%$. We note that particle growth factors due to hydration for aerosol at Grand Canyon National Park, AZ, are reported to be 1.06 at 45–50%, and 1.14 at 50–55% RH (Day and Malm, 2001). The SWYVIS aerosol observed by the PCASP was therefore treated as being dry. In addition, we

adopted the usual assumption of particle sphericity, not thought to introduce significant error (Pilinis and Li, 1998; Collins et al., 2000a).

As the refractive indices of atmospheric aerosol particles and those used for calibration are invariably different, accurate sizing of ambient particles requires that the PCASP calibration be modified subsequent to the experimental observations using refractive indices based on the measured chemical composition of the aerosol. PCASP bin sizes were revised using the diameter scaling method developed by Hand et al. (Hand and Kreidenweis, 1996; Ames et al., 2000). Hand and Kreidenweis (1996) suggest that for refractive indices greater than 1.38, the diameter scaling method does not lead to significant errors in corrected diameter values.

Air sampled through a forward facing inlet mounted above the aircraft boundary layer flow regime, designed for approximately isokinetic sampling at an airspeed of 90 ms^{-1}, was fed to two parallel pairs of 47 mm diameter filters, to collect aerosol material for chemical analysis. The Energy and Environmental Engineering Center at the Desert Research Institute (DRI) in Reno, NV, both prepared the filters and conducted the post-flight analyses. The sequentially mounted filters in channel I were a Gelman PTFE Teflon membrane filter backed by a Pallflex Quartz filter, while those in channel II were a Pallflex Quartz filter backed by a sodium chloride impregnated Whatman 41 cellulose fiber filter. Details of the filter pack system and the standard procedures used for the analyses are documented by Chow et al. (1996) and Watson et al. (2001). They allow for determination of the total mass loading, as well as those of individual elements, ions, and organic and elemental carbonaceous material.

3. Experimental observations

Aerosol, meteorological, and other air chemistry data not reported here, were obtained on 11 flights on seven days having minimal cloud cover, during late morning and early afternoon, in the period 27 February 1996–15 March 1996 (960227–960315). In general, stable conditions were encountered aloft above a lower level mixed layer that deepened during the time period of the flights. Temperatures at the surface (approximately 1900 m msl) were in the range 0 ± 10°C with RH values ranging from 15% to 75%. Aloft, at 5500 m msl, RH values were lower, falling between 15% and 55%.

Daily flight operations originated and terminated in Laramie, WY (41.32°N, 105.67°W), with each flight comprising (i) an initial high-altitude (5500 m msl) westward outbound leg, (ii) a slow zigzag descent (100 m/min) with 80 ± 15 km legs, to the surface, (iii) a series of transverse low-level (75 m agl) legs, (iv) a slow zigzag ascent (100 m/min), with 65 ± 10 km legs, and (v) a concluding eastward high-altitude (5300 m msl) inbound leg. The flights of 10, 11, and 15 March were interrupted by a brief stopover at Rock Springs, WY (41.60°N, 109.07°W). The low-level part of each flight was conducted over the Green River Basin (GRB) of southwest Wyoming, an area of roughly 20,000 km^2 (approximately 41–43°N, 109–110.5°W). This largely uninhabited region contains concentrations of oil and natural gas wells, as well as the 500 km^2 'trona patch', home to five large trona (sodium sesquicarbonate) underground mines. Flight tracks usually followed the same general pattern, except that not every low-level leg was flown on each day.

3.1. Vertical profiles

Fig. 1 (upper panels) shows example descent and ascent profiles of potential temperature (θ), and observed and calculated aerosol scattering coefficient (σ_{scat}), plotted with a vertical resolution of 200 m, for the flights of 29 February and 15 March. Also shown (middle and lower panels) are particle size distributions measured by the PCASP together with the contributions to scattering extinction of particles in each size range, computed by Mie scattering theory as outlined below in Section 4.3, for two altitudes, one high and one low, as specified, for each profile. Descent profiles were conducted in a north–south vertical plane at the same location, downwind of the study region (GRB). Similarly, ascent profiles were carried out in a southeast–northwest vertical plane, upstream of the GRB, and always at the same location. During the profiles, averaged wind directions were westerly. The potential temperature profiles are similar, with θ increasing with height, indicating predominant stability. For the ascent profiles, obtained later in the day, θ varies little at the lowest levels, characteristic of a well-mixed planetary boundary layer that develops during the morning and early afternoon hours. This layer is typically capped by a temperature inversion, above which relative humidities decline rapidly from their values in the PBL, typically 60 ± 15%, to values less than 35%, and sometimes as low as 10%, in the upper two-thirds of the altitude ranges of the profiles.

Within the PBL, number densities of particles ($0.13\,\mu m < D < 3\,\mu m$) are typically about an order of magnitude greater than those higher up, and are relatively uniformly distributed in ascent profiles. In general, number densities were low, sometimes decreasing to 15 cm^{-3} or lower, above the boundary layer. Some profiles, including those of 29 February and the descent profile of 15 March, showed increasing particle number densities above 4400 m. Given the general stability of the atmosphere above the PBL, both these elevated aerosol layers and the 'background' aerosol

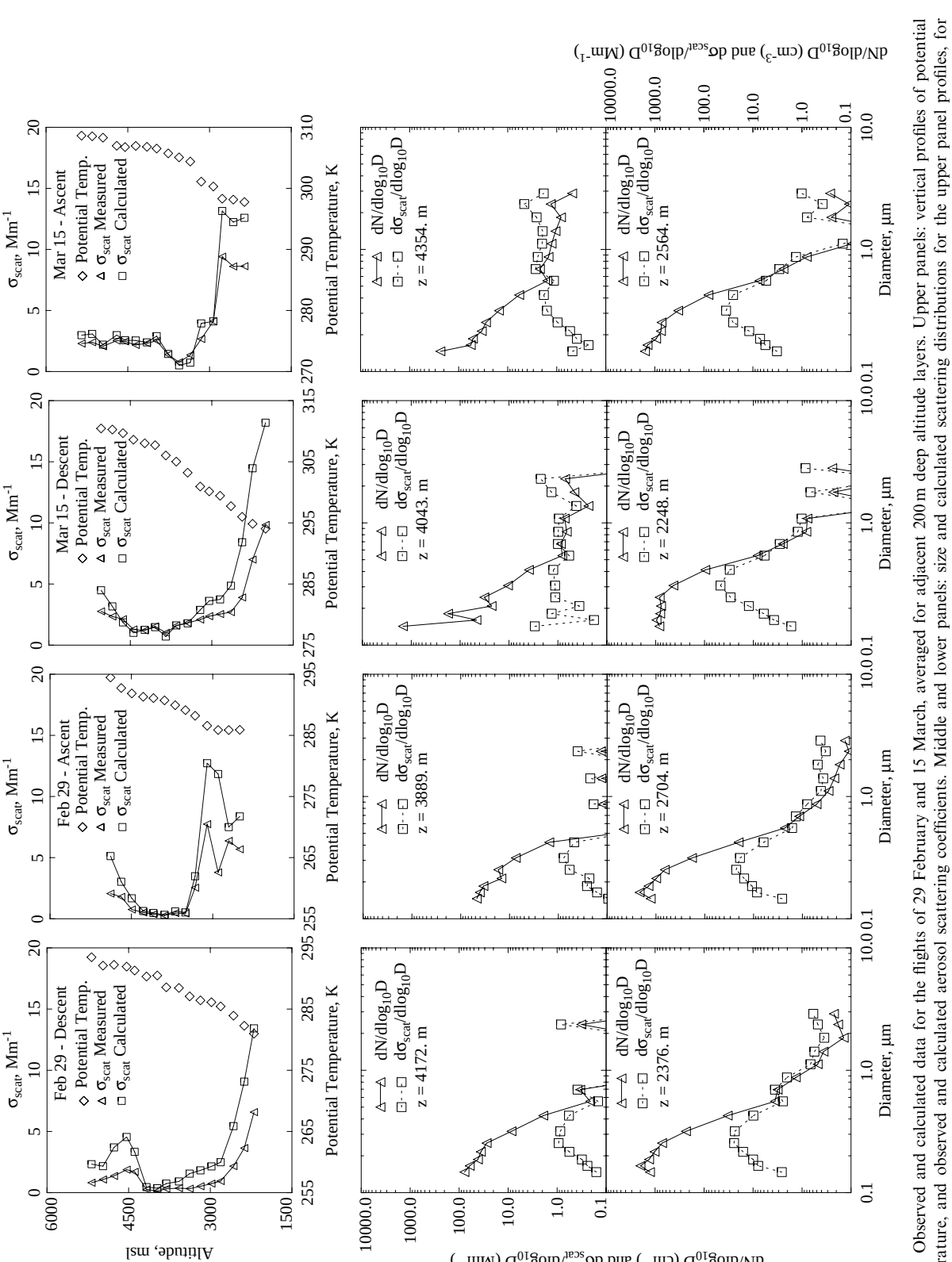

Fig. 1. Observed and calculated data for the flights of 29 February and 15 March, averaged for adjacent 200 m deep altitude layers. Upper panels: vertical profiles of potential temperature, and observed and calculated aerosol scattering coefficients. Middle and lower panels: size and calculated scattering distributions for the upper panel profiles, for specified altitude layers.

aloft must originate well outside the study region and might therefore be expected to contain significant fractions of larger particles. The measured size distributions confirm these expectations (e.g., on 15 March 1996). At lower altitudes the size spectra display typically observed 'roll-off' behavior at particle diameters above about 0.3 μm.

Variations in scattering extinction, measured by the nephelometer, reflect the height dependent changes in aerosol size spectra. Thus extinctions are highest at low altitude and much reduced in the free troposphere. However, higher extinction values again increase in aerosol layers observed above 4400 m. Relative humidity values within the nephelometer chamber were always less than 15%, so that particles generating the observed scattering were presumed to be dry, even when sampled in the PBL.

3.2. Aerosol chemical composition

Chemical composition of the aerosol was assessed through the analyses of the material collected on the filters. The requirements of the analytical protocols coupled with the prevailing low aerosol mass loadings dictated that, in general, only one pair of filters could be exposed per flight. Thus the results represent an integration along flight tracks of between 500 and 1270 km.

Total aerosol mass loadings are shown in Table 1. For individual species, uncertainties often exceed the measured values. They result primarily from the overall low-mass loading of the sampled air, and, possibly, from the adsorption of trace gases on the filter media, and/or the loss of volatile species. The sum of the mass loadings of individual species, measured on the channel II quartz filter, is invariably greater than the gravimetrically determined total mass from the deposit on the channel I Teflon filter, suggesting possible loss of volatile material (Chow et al., 1996; Watson et al., 2001; Watson, 2002). The most abundant ionic species were sulfate and ammonium, with lesser amounts of nitrate, and even smaller amounts of sodium and chloride. The aerosol equilibrium model SEQUILIB (Kim et al., 1993b, c) provides a method for translating ionic concentrations into those of the most thermodynamically stable set of chemical compounds likely to be present in an internally mixed aerosol. The ionic and elemental analyses are consistent with the primary inorganic chemical constituents being $(NH_4)_2SO_4$, $(NH_4)HSO_4$, NH_4NO_3, Na_2SO_4, NH_4Cl, silicates, aluminosilicates, and other mineral species represented by other metal oxides, in addition to organic (OC) and elemental carbon (EC).

3.3. Black carbon

In addition to filter pack measurements of EC, BC was assessed from the aethalometer observations. BC mass concentrations show considerable variability, ranging from a few tens of nanograms per cubic meter in 'clean' air, up to 430 ng m^{-3}. The range of values are at the lower end of those (100–1000 ng m^{-3}) typically found in remote areas of the continental USA (Goldberg, 1985), and may be contrasted to those for urban areas (1000–10,000 ng m^{-3}) and pristine locations (0.5–5 ng m^{-3}) such as the South Pole (Hansen et al., 1988).

BC concentrations calculated for periods when the aircraft was ascending through unpolluted air were often negative, whereas during descent legs they appeared to be anomalously high. Similar behavior has been

Table 1
Filter pack mass loading

Flight	Exposure time (MST)	Mass loading gravimetric (μg m^{-3})	Standard deviation (μg m^{-3})	Mass loading break through (μg m^{-3})	Standard deviation break through (μg m^{-3})
960227	1614–1720	3.95	1.84	0.00	1.80
960229a	1050–1231	0.00	1.24	2.87	1.30
960229b	1235–1407	2.95	1.00	0.00	0.97
960307	0901–1151	1.36	0.93	1.85	0.96
960308	0949–1344	1.97	0.49	0.79	0.49
960310	0858–1109	3.71	0.75	2.15	0.78
960311	0816–1111	3.52	0.57	2.33	0.61
960311	1238–1438	3.36	0.86	1.13	0.86
960315	0841–1115	2.43	0.67	2.79	0.73
960315	1332–1556	1.85	0.69	1.52	0.71

Flights are identified by the date (yymmdd). Suffixes a and b refer to sequentially exposed filter packs on the same flight. Standard deviation error estimates are based on the analytical precision of replicate analyses, field blank concentration uncertainty, and an air sample volume uncertainty of 5%.

Table 2
Aerosol average relative mass concentrations of constituent chemical species

Species	Relative mass (%)
Na_2SO_4	4.2
$(NH_4)_2SO_4 + NH_4HSO_4$	21.2
NH_4Cl	0.4
NH_4NO_3	6.7
Black carbon (BC)	3.8
Organic carbonaceous (OC)	46.7
Mineral	17.1

reported previously for both aethalometer (Bodhaine et al., 1991; Clarke et al., 1997) and Radiance Research particle soot absorption photometer (Sheridan and Ogren, 1999; Collins et al., 2000b) measurements. Pressure induced distortions of the filters within the instruments are suspected to underlie the observed behavior (Hansen, 2002). BC concentrations are therefore only considered valid during periods of level flight.

Combining the BC concentrations from the aethalometer measurements with those of the other chemical species from the filter pack measurements (excluding EC) allows the percentage contribution of each species to the total mass of the aerosol to be calculated. When averaged over all samples, the percentages shown in Table 2 are obtained.

3.4. Observed aerosol optical properties

Three minute average values of scattering and absorption extinctions, and single scatter albedo (SSA), derived from the nephelometer and aethalometer measurements carried out during 2 h low-altitude (75 m agl) flight segments on 8, 10, and 15 March 1996, are shown in Fig. 2. Also plotted are calculated values, based on 3 min size distribution averages, of scattering extinction and truncation correction factor (TCF), computed by Mie theory as described below (Section 4.3). The TCF is the ratio of the scattering extinctions computed by the Mie theory algorithm for the angular ranges 0–180° and 9–168° (the viewing angle of the nephelometer), using both refractive index values and size distribution parameters specific to the observational data. Multiplying the observed scattering extinction by the TCF allows a scattering extinction for the 0–180° range to be estimated.

The upper panel of Fig. 2, for 8 March illustrates data during a period of relatively unpolluted northwesterly flow, characterized by observed σ_{scat} values $<4.5\,Mm^{-1}$. Periods of 'clean' air were also encountered during other low-level flight segments, including those on 10 and 15 March but they were punctuated by regions that exhibit higher extinction values. On these days winds within the GRB were southwesterly and weaker than on 8 March. The values of absorption extinction (σ_{abs}) were calculated using a value for the absorption cross section of suspended BC particles at 530 nm of $10\,m^2\,g^{-1}$ (Moosmüller et al., 1998). SSA, the fraction of the total extinction due to scattering, was determined from

$$SSA = (\sigma_{scat})/(\sigma_{scat} + \sigma_{abs}).$$

The plots show that intervals of higher scattering and absorption are essentially coincident, so that SSA values do not appear to vary systematically with scattering (or absorption) extinction. Low-level flight average SSA values typically fall in the range 0.7–0.9.

4. Optical closure

The SWYVIS aerosol measurements provide an opportunity to carry out an optical 'closure experiment' in which computed extinctions are compared to those measured directly. Thus for each flight the derived chemical composition of the particulates is used to compute an aerosol refractive index value which is, in turn, used both to revise the aerosol size distributions determined by the PCASP, and, subsequently, to calculate aerosol total extinctions using Mie theory for comparison with the extinctions derived from the nephelometer and aethalometer observational data, in both clean and polluted regions of the PBL, and in the free troposphere.

4.1. Aerosol size distribution

The SWYVIS aerosol size data were fitted to bimodal lognormal number distributions, yielding numerical values of the total number density (n_i), geometric diameter (D_i), and geometric standard deviation (σ_i) for accumulation ($i = 1$) and coarse ($i = 2$) modes. For some scattering calculations, the distributions were extrapolated over the diameter range 0.02–10 μm, so that contributions to scattering from particles both smaller and larger than those detected by the PCASP ($0.13\,\mu m < D < 3\,\mu m$) could be included.

4.2. Refractive index values

Refractive indices were calculated for an assumed internally mixed dry aerosol, using the partial molar refraction method (Stelson, 1990). BC was assigned a refractive index value of 1.96–0.66*i* (Hasan and Dzubay, 1983) while a value of 1.4583–0*i* was used for OC (Hasan and Dzubay, 1983; Stelson, 1990). Refractive indices of other relevant species are commonly available. The volume weighted refractive index method (Hasan and Dzubay, 1983; Ouimette and Flagan, 1982) was used to include the imaginary part of the refractive index.

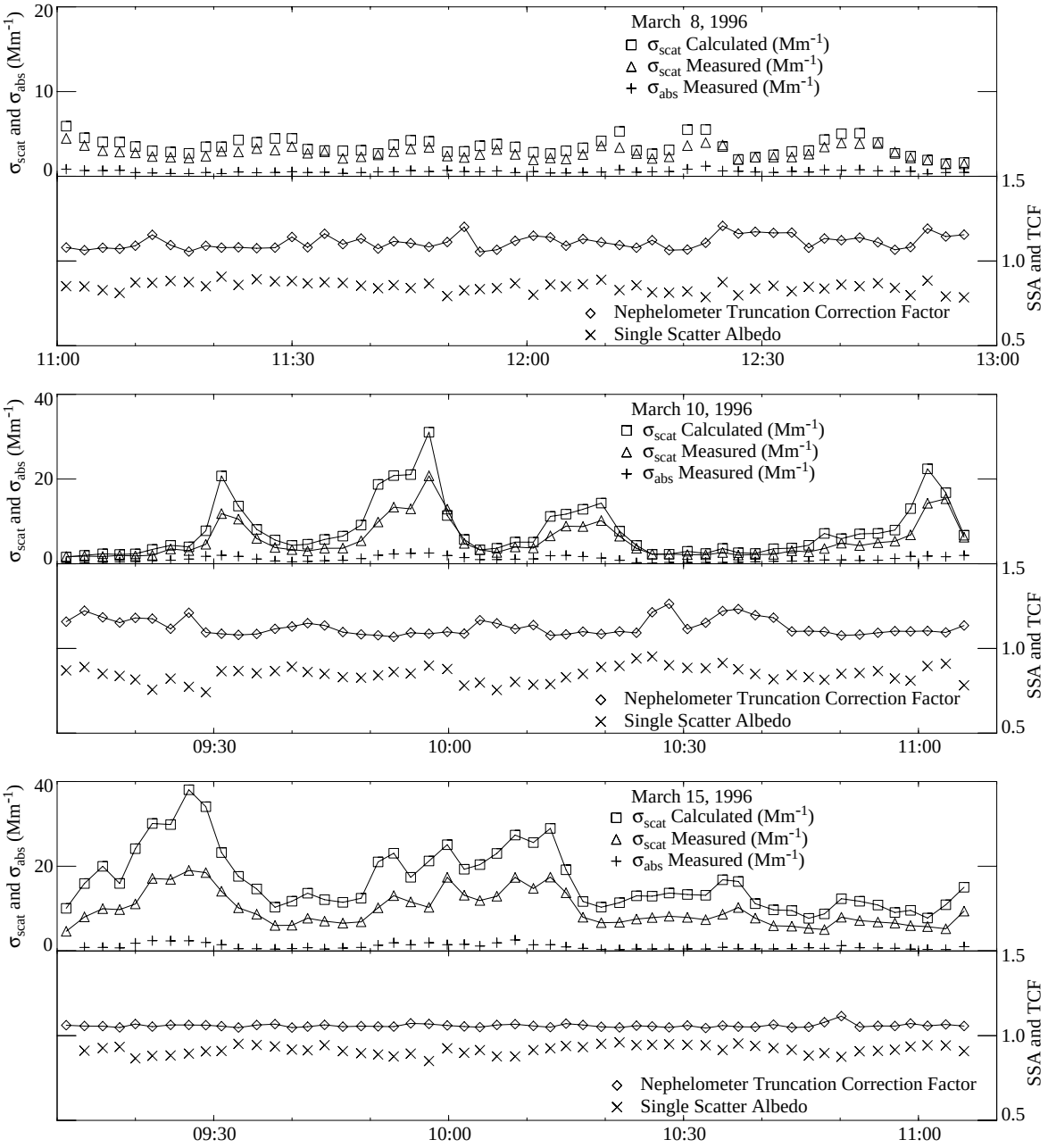

Fig. 2. Variation with local time (MST) of three minute averaged values of scattering extinction (observed and calculated), absorption extinction, single scatter albedo, and nephelometer truncation correction factor at low-altitude for flights of 8 March (upper panel), 10 March (middle panel), and 15 March (lower panel).

Applying the assumption of homogeneous internal mixing to heterogeneously mixed particles may overestimate the extent of absorption (Fuller et al., 1999), thereby augmenting other errors arising from uncertainties in the chemical composition, and in the assumed refractive index of the organic component.

Numerical values of refractive index were calculated after apportioning the non-BC aerosol mass, obtained by subtracting the aethalometer-derived BC mass from the total aerosol mass, determined as the sum of that determined from the gravimetric analysis of the channel I Teflon filter and the 'break through' mass on the

channel I back-up quartz filter, according to the relative proportions of the chemical components in the mixture. Table 3 shows the computed refractive index values for each flight.

4.3. Optical properties calculation

Aerosol optical properties were calculated using Mie scattering routines based on that of Bohren and Huffman (1983) using both the recalibrated PCASP aerosol size histogram and the bimodal lognormal fits, together with the aerosol complex index of refraction. Scattering coefficients were obtained by integrating the Mie phase function over the angular ranges 9–168°, corresponding to the restricted field of view of the nephelometer, and 0–180°. The calculated contributions to scattering extinction of particles in each of the 15 size 'bins' measured by the PCASP are shown in the eight lower panels of Fig. 1, for specified altitudes. The calculations show that in the PBL the largest contributions are from particles around 0.3 μm, whereas in the free troposphere, contributions from particles of all sizes observed by the PCASP can be significant (e.g., on 15 March). Computed scattering extinctions integrated across the entire particle size range detected by the PCASP are plotted as a function of altitude in the upper panels of Fig. 1 and as a function of time in Fig. 2. Inspection of Fig. 1 shows that agreement with the observed σ_{scat} values is generally very good aloft when scattering extinctions are small, but is less satisfactory both at lower altitudes and in higher density aerosol layers above 4400 m msl. Similarly, Fig. 2 shows that computed and observed values of σ_{scat} agree reasonably well in low altitude regions where scattering extinctions are small (e.g., on 8 March from 12:42–12:52 and from 10:25 to 10:45 on 10 March) but elsewhere computed values exceed those that are observed.

Table 3
Computed refractive index

Flight	Refractive index
960227	1.5363–0.0276*i*
960229a	1.4865–0.0272*i*
960229b	1.4986–0.0209*i*
960307	1.4766–0.0079*i*
960308	1.5037–0.0162*i*
960310am	1.4936–0.0137*i*
960311am	1.5354–0.0203*i*
960311pm	1.5556–0.0266*i*
960315am	1.5306–0.0179*i*
960315pm	1.4944–0.0158*i*

Aerosol scattering and total extinctions were also computed using the bimodal lognormal fits of the PCASP spectra averaged over 40 constant-altitude flight segments, ranging from 5 to 55 min. The shortest time periods (<10 min) were usually segments of elevated extinction. Selection criteria for the averaging intervals included the presence or absence of plumes, as identified by observed particle number densities and scattering extinction, and whether chosen segment locations were visited by the aircraft more than once during the same flight.

Table 4 shows the bimodal lognormal fitting parameters for PBL segments on two representative flights. The values of geometric diameter (D) and geometric standard deviation (σ) for each mode display uniformity both overall and for each flight. Very similar values are

Table 4
Bimodal size distribution parameters for flights 960310 and 960315

Time interval	Segment	n_1 (cm^{-3})	D_1 (μm)	σ_1	n_2 (cm^{-3})	D_2 (μm)	σ_2
960310							
0920–0940	10C	650	0.124	1.61	0.55	1.00	2.47
0929–0934	10E	1157	0.128	1.60	1.15	0.72	2.25
0940–1005	10F	748	0.134	1.60	0.90	0.78	2.32
0951–0959	10G	1140	0.14	1.60	1.72	0.70	2.23
1012–1020	10J	1180	0.122	1.61	0.95	0.74	2.31
1025–1040	10K	141	0.132	1.61	0.49	0.96	2.51
1050–1110	10M	785	0.126	1.61	0.88	0.82	2.38
960315							
0915–1115	15C	716	0.134	1.60	0.45	0.82	2.20
0920–0930	15D	1175	0.142	1.60	1.07	0.74	2.20
0930–0955	15E	739	0.130	1.60	0.34	0.92	4.38
0955–1005	15F	817	0.138	1.60	0.50	0.90	2.25
1005–1010	15G	966	0.142	1.60	0.52	1.08	2.28
1015–1045	15H	647	0.128	1.60	0.31	0.82	2.20
1045–1115	15J	493	0.134	1.59	0.43	0.80	2.19

found on other days. Segments 10G, 10E, and 10J on 10 March are non-chronological, sequentially downwind, plume transects, spaced approximately 30–40 km apart. Transects of this plume are apparent in the upper half of the middle panel of Fig. 2, as indicated by higher scattering extinctions, in contrast to those for segment 10 K, also shown in Fig. 2, located in less polluted air. Similar size spectra were encountered five days later during the flight on 15 March (Fig. 2, lower panel). On this flight the aircraft visited the same location at both 09:26 and 10:08 during segments 15D and 15G, observing 2-min average PCASP particle number densities of 880 and 741 cm^{-3}, respectively. Similarly, flight tracks between 09:42–09:47 and 10:38–10:43 (during 15E and 15H) were coincident. Measured 2-min particle number densities during these periods were 363 and 335 cm^{-3}. These pairs of values give an indication of the temporal variability of particle loadings. While the fitted number densities for each of these intersections show variations of about 20%, the accumulation mode diameters (D_1) are identical within 1%. Other differences in number density, size distribution, and scattering extinction may result from both variability in the size (D_2) and concentration (n_2) of larger particles and adjacent track sections having different particle loadings being included in these segment time intervals.

Table 5 gives bimodal size distribution parameters for representative flight segments in both 'clean' surface air and in the free troposphere. All of the tabulated low altitude time intervals are included in the time series plots shown in Fig. 2. Particle number densities aloft ($z > 3000$ m msl) are significantly lower than those at the surface, with total concentrations measured by the PCASP frequently falling well below 100 cm^{-3}. An exception occurs during flight segment 29L, where the elevated aerosol layer previously observed above 4400 m msl in the descent sounding (Fig. 1) was again sampled, but at a different location. The table shows that geometric diameters and standard deviation values are in the same range and depict no obvious discernable variability pattern with altitude.

Fig. 3 shows scatter plots of scattering and total extinction, together with a plot of the ratio of calculated to observed SSA vs. observed SSA for the 46 flight segments selected. The scatter plots for both scattering and total extinction can be fitted by linear relationships, but with slopes of best-fit lines that differ significantly from unity. Calculated total extinctions are invariably greater than those observed, by $53 \pm 20\%$. Analogous plots (not shown) using calculated extinctions for particles in the diameter range 0.02–4.0 μm reduce the disparity to $42 \pm 20\%$. While the data points on the SSA plot display considerable scatter, they define a linear relationship of negative slope.

5. Discussion

Success in closure experiments depends on both the quality of the experimental data and the validity of the computational assumptions. Studies based on surface data, obtained under relatively slowly changing atmospheric conditions, can often utilize long-term averages, thereby reducing experimental uncertainties. For airborne investigations, however, conditions may change significantly within a few seconds, and measurement periods are invariably limited by the length of the flight to a few hours. In this study, being restricted to a single set of aerosol chemical analyses for an entire flight limits both our ability to discern changing chemical composition and aerosol refractive index along the flight track in the PBL and in the free troposhere and, consequently, the degree to which optical closure can be achieved. The difficulties are exacerbated by low-mass loadings, which result in barely acceptable signal-to-noise ratios for the

Table 5
Bimodal size distribution parameters for high altitude and surface 'clean' air in the planetary boundary layer

Flight	Time	Altitude (m msl)	Segment	n_1 (cm^{-3})	D_1 (μm)	σ_1	n_2 (cm^{-3})	D_2 (μm)	σ_2
960229	1028–1117	5500	29A	154	0.120	1.61	0.18	0.96	2.60
960229	1350–1426	5150	29L	436	0.136	1.60	0.47	1.38	2.28
960308	1335–1400	5250	8P	49	0.116	1.62	0.23	0.82	2.53
960315	0815–0835	5400	15A	134	0.098	1.61	0.47	1.04	2.48
960315	1512–1532	5300	15R	102	0.122	1.62	1.38	1.09	2.50
960315	1532–1551	5300	15V	124	0.122	1.61	0.26	1.24	2.42
960308	1125–1140	2000	8G	413	0.112	1.60	0.23	1.16	2.41
960308	1140–1200	2100	8H	385	0.114	1.60	0.23	1.02	2.43
960308	1220–1240	2000	8L	260	0.126	1.60	0.34	1.06	2.42
960308	1240–1300	2350	8M	233	0.122	1.61	0.22	1.04	2.46
960310	1025–1040	2175	10K	141	0.132	1.61	0.49	0.96	2.51
960310	1040–1050	2100	10L	412	0.120	1.60	0.72	0.64	2.22

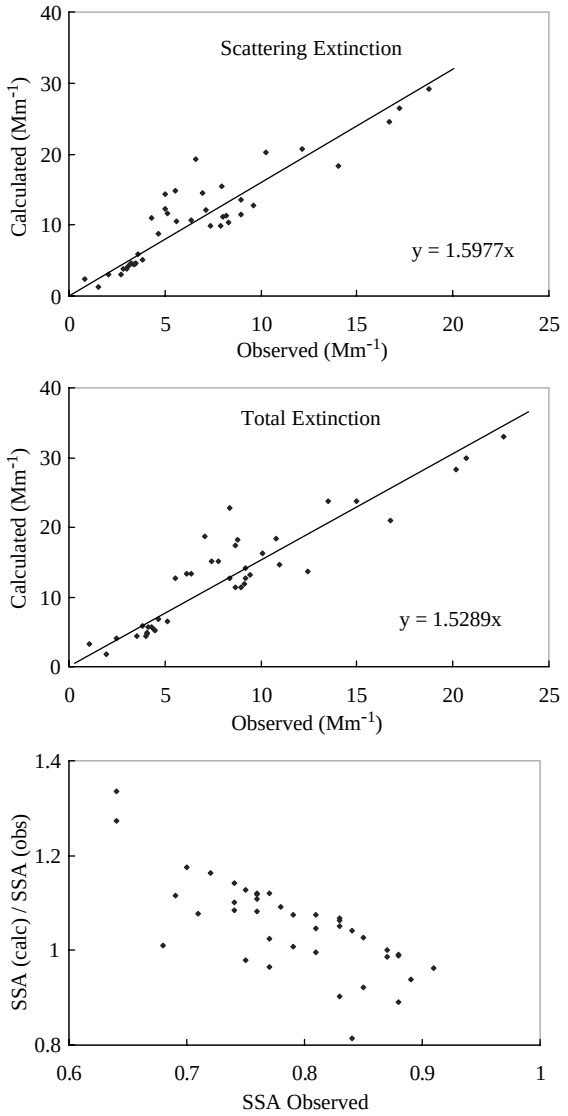

Fig. 3. Aerosol scattering extinction, total extinction, and single scatter albedo: calculated and observed values.

analytical data, thereby increasing uncertainties considerably.

Notwithstanding these difficulties, the results show that both the mass loading and relative distribution of non-mineral aerosol components are similar to those found at surface sites in the northern Rocky Mountain region (Watson et al., 2001; Malm et al., 2000) with OC and sulfates dominating the mixture. Bimodal size distributions adequately describe observed SWYVIS size distributions, and display slight broadening of the coarse mode with increasing altitude. In the accumulation mode, median particle diameters and geometric standard deviations (Tables 4 and 5) are very similar to those reported by Kim et al. (1993a) and Pinnick et al. (1993). For the coarse mode, however, both inter- and intrastudy comparisons of the diameters show slightly more variability, though modal standard deviations are comparable.

Distributions with a higher fraction of larger particles such as those at higher altitudes plotted in Fig. 1, result in more equal contributions to extinction across the PCASP size range. Similarly, these distributions have higher TCF values that reflect higher percentage contributions of forward scattering to extinction. While TCF values plotted in Fig. 2 range up to 1.27, most of the lowest values are found for regions where scattering extinction is elevated, as seen in the plots for 10 and 15 March. These regions are downwind of pollutant sources, suggesting that they may be influenced by local sources of relatively small particles.

While both calculated scattering and total extinctions are linearly related to the corresponding observed extinctions, as shown in Fig. 3, they exceed the measured values by an average of 60% and 53%, respectively. Analogous plots for individual flights (not shown) also display a linear correlation between calculated and observed values, but with slopes ranging from 1.29 to 1.90 ($r^2 > 0.95$). Thus data from different flights are internally self-consistent on a per flight basis and do not scatter randomly around the best-fit lines in Fig. 3 plots. However, as Figs. 1 and 2 demonstrate, degrees of agreement vary within each flight, with ratios of calculated to observed scattering extinctions ranging from unity to a factor of two.

The 3-min average SSA values derived from the nephelometer and aethalometer measurements plotted in Fig. 2 show variations of ± 0.1. For the selected 40 flight segments, observed SSA values average 0.791 with a standard deviation of 0.064. The average of the ratio of calculated to observed SSA values (SSA_{calc}/SSA_{obs}) is 1.05 ± 0.10. Fig. 3 shows that SSA_{calc}/SSA_{obs} decreases with increasing SSA_{obs}. This trend results from the use of a single refractive index value, based on an average aerosol chemical composition for each flight. Thus, calculated absorption coefficients are overestimated for flight segments having actual BC aerosol contributions lower than the average, leading to underprediction of SSA, and vice versa. In contrast to the calculated values, observed values of SSA are based on segment specific BC mass loadings. Thus while SSA_{calc} and SSA_{obs} are in reasonable agreement when averaged over all flight segments, SSA_{calc} is overestimated for aerosols for which SSA_{obs} is low, and underestimated for those with a high SSA_{obs}. In addition, use of a single refractive index for all particles in each size spectrum presumes that the BC mass fraction is the same for particles of different sizes, a dubious assumption given that BC is predominantly found in smaller particles (McMurry and Zhang, 1989). The contribution to absorption extinction from larger particles may therefore be overestimated.

Not unexpectedly, calculated SSA values display a decreasing trend as the relative contribution to absorption extinction from larger particle increases. When particles in the accumulation mode dominate absorption extinction, calculated SSA values increase, approaching a limiting value of 0.87 ± 0.03.

Optimization of the agreement between calculated extinctions and those observed in airborne studies requires particle size distribution, and refractive index values that are both spatially and temporally resolved, criteria that are not met for SWYVIS. Of necessity, average refractive index values have been used to analyze data from flight segments where their applicability is questionable, and, consequently, revised PCASP bin sizes and computed scattering extinctions may not be wholly accurate. However, the internal consistency of the scatter plot data for individual flights, coupled with the absence of any obvious correlation between the slope of those plots and refractive index, suggests that inaccuracies in refractive index values and by implication underlying uncertainties in the aerosol chemical composition, cannot explain the observed discrepancies between the calculated and observed extinction values in any simple way, even though they may contribute to them. For declining 'real' refractive index values, PCASP bin size calibrations shift to larger sizes, leading to revised aerosol size distributions that tend to increase calculated scattering. This effect is partially offset, however, by reduced scattering resulting from the lower refractive index. Moreover, it implies that if the particles observed by the PCASP were partially hydrated, contrary to our assumption then calculated scattering coefficients would be larger and agreement in the closure experiment worsened.

The PCASP derived SWYVIS aerosol size distributions were extrapolated for the Mie calculations shown in Fig. 3, to include contributions to extinction from particles presumed to be present but not detected. Omitting this extrapolation reduces calculated extinction values, but as Figs. 1 and 2 show, calculated extinctions based on the unfitted PCASP size distributions often exceed those observed. Overestimation of particle concentrations would clearly enhance computed scattering coefficients, and cannot be excluded as a plausible error in this data set, but the magnitude of this uncertainty remains unknown. Such an error would need to result from overestimation of the number of particles larger than the minimum size detected by the PCASP since scattering contributions from particles smaller than this are thought to be minimal (Liu and Daum, 2000). The results shown in Fig. 1 corroborate this assertion.

Observational errors associated with the nephelometer measurements may be important. Here two principal issues are apparent, the first concerning particle hydration, and the second, particle loss during sampling. Ambient RH values during the flights ranged from 15% to 75% in the PBL, and were generally less than 35% in the free troposhere. Corresponding ambient temperatures were usually in the range $0^\circ \pm 10^\circ C$ and $< -15^\circ C$, respectively. While some hydration of the aerosol might be anticipated at higher RH values (Tang, 1996; Day et al., 2000; Gasso et al., 2000; Day and Malm, 2001), the low RH ($<15\%$) within the nephelometer inside the aircraft would ensure that particles would be effectively dried. Warming of the sampled airstream could also result in a shift in size distribution to lower sizes as a result of partial or total volatilization of some particles (Bergin et al., 1997; Watson, 2002), resulting in a reduced scattering signal. Were observed scattering extinctions to have been as high as those calculated, the average observed SSA value would become 0.85 ± 0.05, and the ratio of calculated to observed SSA would fall to 0.97 ± 0.07.

Modification of particle size distributions in the air sampled by the nephelometer might therefore go some way towards explaining differences between observed and calculated extinctions. However, if loss of volatile material from particles did indeed take place, it cannot have occurred uniformly throughout the flights, as agreement between observed and computed extinctions shows considerable variability. This conclusion hints at the possibly varying chemical composition of the aerosol. In the absence of further information, resolution of this issue currently remains enigmatic.

6. Summary

As part of the Southwest Wyoming Visibility Study (SWYVIS), in situ measurements of aerosol size distribution, chemical composition, and scattering extinction and absorption have been carried out using the Wyoming King Air research aircraft, both at ca. 75 m above the surface and in the middle troposphere, over the Green River basin of Wyoming. In the free troposphere, particle number densities were generally low, resulting in contributions to total extinction that were significantly less than that of Rayleigh scattering. Even at low altitudes, the aircraft often encountered regions of minimally contaminated air, occasionally punctuated by pollutant plumes, coincidentally detected by the PCASP, nephelometer and aethalometer, when downwind of local emission sources. Subsequent observations at locations sampled earlier on the same flight revealed little temporal variability. Vertical profiles were obtained that characterized scattering extinction in the PBL and in the stable free troposphere.

Analyses of bulk aerosol filter samples collected on each flight showed that the average chemical composition of the particulates was similar to that observed in other studies conducted in relatively unpopulated areas

of the Rocky Mountain region of the western USA, being dominated by organic carbonaceous material. Sulfates and refractory materials were the largest inorganic contributors. Refractive indices were calculated from the aerosol chemical compositions determined for each flight and used, first, to revise particle size distributions measured by the PCASP, and, subsequently, to compute aerosol extinctions.

The data have been used to attempt a closure experiment in which computed extinctions have been compared to those derived from nephelometer and aethalometer observations, both along the flight track and for vertical profiles, and for 40 selected flight segments. Particle populations in those segments were fitted to bimodal lognormal size distributions. While values of geometric diameter and geometric standard deviation are very similar for the accumulation mode at all altitudes, the corresponding coarse mode values show somewhat greater variability, and lead to greater contributions to extinction by larger particles aloft.

The overall average ratio of computed to measured SSA was 1.05, with a standard deviation of 0.10. Calculated extinctions are linearly correlated with those that are observed both for individual flights and for the data set as a whole. When averaged over all flights, the ratio of calculated to observed total extinction, after correction for nephelometer truncation error, is 1.53, but this factor varies for individual flights from 1.29 to 1.90. This is in contrast to most other optical closure studies, where calculated extinctions are usually smaller than those observed. Aside from computational assumptions, various factors may additionally contribute to the uncertainties that lead to the discrepancy, including those associated with the characterization of size distributions and chemical compositions of the aerosol, but their influence is obscure. Partial or total vaporization of volatile material, thereby compromising the integrity of the sampled aerosol, may possibly lead to reduced observed extinctions. The underlying cause of discrepancies between observed and computed extinctions, however, remains uncertain.

Acknowledgements

We are indebted to our pilot, Ernie Gasaway, and to Perry Wechsler and all the other members of the UW DAS technical support team, unfortunately too numerous to mention individually, whose dedication and hard work made the airborne phase of this project possible. Thanks are also due to Peter Liu for help with Mie scattering routines. We also gratefully acknowledge financial support from the EPA EPSCoR program, Project No. R821842-01-0, a consortium of industrial organizations operating in the Green River basin of Wyoming, both the Department of Environmental Quality and the Science, Technology, and Energy Authority of the State of Wyoming, and the Research Office of the University of Wyoming.

References

Ames, R.B., Hand, J.L., Kreidenweis, S.M., Day, D.E., Malm, W.C., 2000. Optical measurements of aerosol size distributions in Great Smoky Mountains National Park: dry aerosol characterization. Journal of the Air and Waste Management Association 50, 665–676.

Bates, T.S., Huebert, B.J., Gras, J.L., Griffiths, F.B., Durkee, P.A., 1998. International Global Atmospheric Chemistry (IGAC) project's first aerosol characterization experiment (ACE 1): overview. Journal of Geophysical Research 103, 16297–16318.

Bergin, M.H., Ogren, J.A., Schwartz, S.E., McInnes, L.M., 1997. Evaporation of ammonium nitrate aerosol in a heated nephelometer: implications for field measurements. Environmental Science and Technology 31, 2878–2883.

Bodhaine, B., DeLuisi, J., Boatman, J., Kim, Y., Wellman, D., Gunter, R.L., Post, M.J., Cupp, R., McNice, T., Rosen, J., Sheridan, P., Schnell, R., Garvey, D., Wade, A., Steinhoff, R., 1991. The second Front Range Lidar, Aircraft, Balloon experiment. NOAA data report ERL CMDL-8.

Bohren, C.F., Huffman, D.R., 1983. Absorption and Scattering of Light by Small Particles. John Wiley, New York.

Chow, J.C., Watson, J.G., Lu, Z., Lowenthal, D.H., Frazier, C.A., Solomon, P.A., Thuillier, R.H., Magliano, K., 1996. Descriptive analysis of PM2.5 and PM10 at regionally representative locations during SJVAQS/AUSPEX. Atmospheric Environment 30, 2079–2112.

Clarke, A.D., Porter, J.N., Valero, F.P.J., Pilewskie, P., 1996. Vertical profiles, aerosol microphysics, optical closure during the Atlantic stratocumulus transition experiment: measured and modelled column optical properties. Journal of Geophysical Research 101, 4443–4453.

Clarke, A.D., Uehara, T., Porter, J.N., 1997. Atmospheric nuclei and related aerosol fields over the Atlantic: clean subsiding air and continental pollution during ASTEX. Journal of Geophysical Research 102, 25281–25292.

Collins, D.R., Jonsson, H.H., Seinfeld, J.H., Flagan, R.C., Gassó, S., Hegg, D.A., Russell, P.B., Schmid, B., Livingston, J.M., Öström, E., Noone, K.J., Russell, L.M., Putaud, J.P., 2000a. In situ aerosol size distributions and clear-column radiative closure during ACE-2. Tellus 52B, 498–525.

Collins, D.R., Jonsson, H.H., Liao, H., Flagan, R.C., Seinfeld, J.H., Noone, K.J., Hering, S.V., 2000b. Airborne analysis of the Los Angeles aerosol. Atmospheric Environment 34, 4155–4173.

Cowling, E.B., Chameides, W.L., Kiang, C.S., Fehsenfeld, F.C., Meagher, J.F., 1998. Introduction to special section: the Southern Oxidants Study Nashville/Middle Tennessee ozone study. Journal of Geophysical Research 103, 22209–22212.

Day, D.E., Malm, W.C., Kreidenweis, S.M., 2000. Aerosol light scattering measurements as a function of relative

humidity. Journal of the Air and Waste Management Association 50, 710–716.

Day, D.E, Malm, W.C., 2001. Aerosol light scattering measurements as a function of relative humidity: a comparison between measurements made at three different sites. Atmospheric Environment 35, 5169–5176.

de Reuss, M., Krejci, R., Williams, J., Fischer, H., Scheele, R., Ström, J., 2001. Vertical and horizontal distributions of the aerosol number concentration and size distribution over the northern Indian Ocean. Journal of Geophysical Research 106, 28629–28641.

Fuller, K.A., Malm, W.C., Kreidenweis, S.M., 1999. Effects of mixing on extinction by carbonaceous particles. Journal of Geophysical Research 104, 15941–15954.

Gasso, S., Hegg, D.A., Covert, D.S., Collins, D., Noone, K.J., Öström, E., Schmid, B., Russell, P.B., Livingston, J.M., Durkee, P.A., Jonsson, H., 2000. Influence of humidity on the aerosol scattering coefficient and its effect on the upwelling radiance during ACE-2. Tellus 52B, 546–567.

Goldberg, E.D., 1985. Black Carbon in the Environment. John Wiley, New York.

Gundel, L.A., Dodd, R.L., Rosen, H., Novakov, T., 1984. The relationship between optical attenuation and black carbon concentration for ambient source particles. Science of the Total Environment 36, 197–202.

Gunter, R.L., 1994. Characterization of the optical properties of California aerosols during the San Joaquin Valley Air Quality Study/Atmospheric Utility Signatures, Predictions, and Experiments (SJVAQS/AUSPEX). MS Thesis, University of Wyoming.

Gunter, R.L., Hansen, A.D.A., Boatman, J.F., Bodhaine, B.A., Schnell, R.C., Garvey, D.M., 1993. Airborne measurements of airborne optical properties over south-central New Mexico. Atmospheric Environment 27A, 1363–1368.

Hand, J.L., Kreidenweis, S.M., 1996. Size corrections based on refractive index for Particle Measuring Systems Active Scattering Aerosol Spectrometer Probe; CIRA report, ISSN No. 0737-5352-31, Colorado State University, Fort Collins, CO.

Hansen, A.D.A., 2002. Personal communication.

Hansen, A.D.A., Rosen, H., Novakov, T., 1984. The aethalometer—an instrument for the real-time measurement of optical absorption by aerosol particles. Science of the Total Environment 36, 191.

Hansen, A.D.A., Bodhaine, B.A., Dutton, E.G., Schnell, R.C., 1988. Aerosol black carbon measurements at the South Pole: initial results, 1986–1987. Geophysical Research Letters 15, 1193–1196.

Hartley, W.S., Hobbs, P.V., Ross, J.L., Russell, P.B., Livingston, J.M., 2000. Properties of aerosols aloft relevant to direct radiative forcing off the mid-Atlantic coast of the United States. Journal of Geophysical Research 105, 9859–9885.

Hasan, H., Dzubay, T.G., 1983. Apportioning light extinction coefficients to chemical species in atmospheric aerosol. Atmospheric Environment 17, 1573–1581.

Hegg, D.A., Hobbs, P.V., Gassó, S., Nance, J.D., Rango, A.L., 1996. Aerosol measurements in the Arctic relevant to direct and indirect radiative forcing. Journal of Geophysical Research 101, 23349–23363.

Hegg, D.A., Livingston, J., Hobbs, P.V., Novakov, T., Russell, P., 1997. Chemical apportionment of aerosol column optical depth off the mid-Atlantic coast of the United States. Journal of Geophysical Research 102, 25293–25303.

Husar, R.D., Prospero, J.M., Stowe, L.L., 1997. Characterization of tropospheric aerosols over the oceans with the NOAA advanced very high resolution radiometer optical thickness operational product. Journal of Geophysical Research 102, 16899–16909.

Kim, Y.J., Boatman, J.F., Gunter, R.L., Wellman, D.L., Wilkison, S.W., 1993a. Vertical distribution of atmospheric aerosol size distribution over south-central New Mexico. Atmospheric Environment 27A, 1351–1362.

Kim, Y.P., Seinfeld, J.H., Saxena, P., 1993b. Atmospheric gas-aerosol equilibrium. I Thermodynamic model. Aerosol Science and Technology 19, 157–181.

Kim, Y.P., Seinfeld, J.H., Saxena, P., 1993c. Atmospheric gas-aerosol equilibrium. II. Analysis of common approximations and activity coefficient calculation methods. Aerosol Science and Technology 19, 182–198.

Liu, P.S., Leaitch, W.R., Strapp, J.W., Wasey, M.A., 1992. Response of particle measuring systems airborne ASASP and PCASP to NaCl and latex particles. Aerosol Science and Technology 16, 83–95.

Liu, Y., Daum, P., 2000. The effect of refractive index on size distributions and light scattering coefficients derived from optical particle counters. Journal of Aerosol Science 31, 945–957.

Malm, W.C., Pitchford, M.L., Scruggs, M., Sisler, J.F., Ames, R., Copeland, S., Gebhart, K.A., Day, D., 2000. Spatial and seasonal patterns and temporal variability of haze and its constituents in the United States. ISSN: 0737-5352-47. Cooperative Institute for Research in the Atmosphere, Colorado State University, Fort Collins, CO.

McMurry, P.H., Zhang, X.Q., 1989. Size distribution of ambient organic and elemental carbon. Aerosol Science and Technology 10, 430–437.

Moosmüller, H., Arnott, W.P., Rogers, C.F., Chow, J.C., Frazier, C.A., 1998. Photoacoustic and filter measurements related to aerosol light absorption during the Northern Front Range Air Quality Study (Colorado 1996/1997). Journal of Geophysical Research 103, 28149–28157.

Öström, E., Noone, K.J., 2000. Vertical profiles of aerosol scattering and absorption measured in situ during the North Atlantic Characterization Experiment (ACE-2). Tellus 52B, 526–545.

Ouimette, J.R., Flagan, R.C., 1982. The extinction coefficient of multicomponent aerosols. Atmospheric Environment 16, 2405–2419.

Peseva, P., Horvath, H., Kasahara, M., 2001. A local optical closure experiment in Vienna. Journal of Aerosol Science 32, 1249–1267.

Philippin, S., Neusüß, Wiedensohler, A., Heintzenberg, J., Carrico, C.M., Rood, M.J., 1998. Optical properties of anthropogenically influenced aerosols in a marine atmosphere: an optical closure experiment. Journal of Aerosol Science 29 (Suppl. 1), S1151–S1152.

Pilinis, C., Li, X., 1998. Particle shape and internal inhomogeneity effects on the optical properties of tropospheric aerosols of relevance to climate forcing. Journal of Geophysical Research 103, 3789–3800.

Pinnick, R.G., Fernandez, G., Martinez-Andaloza, E., Hinds, B.D., Hansen, A.D.A., Fuller, K., 1993. Aerosol in the arid southwestern United States: measurements of mass loading, volatility, size distribution, absorption characteristics, black carbon content and vertical structure to 7 km above sea level. Journal of Geophysical Research 98, 2651–2666.

Quinn, P.K., Marshall, S.F., Bates, T.S., Covert, D.S., Kapustin, V.N., 1995. Comparison of measured and calculated aerosol properties relevant to the direct radiative forcing of tropospheric sulfate aerosol on climate. Journal of Geophysical Research 100, 8977–8991.

Quinn, P.K., Coffman, D.J., 1998. Local closure during the First Aerosol Characterization Experiment (ACE 1): Aerosol mass concentration and scattering and backscattering coefficients. Journal of Geophysical Research 103, 16547–16596.

Raga, G.B., Jonas, P.R., 1995. Vertical distribution of aerosol particles and CCN in clear air around the British Isles. Atmospheric Environment 29, 384–673.

Rosen, J.M., Bodhaine, B.A., Boatman, J.F., DeLuisi, J.J., Kim, Y., Post, M.J., Sheridan, P.J., Schnell, R.C., Garvey, D.M., 1992. Measured and calculated optical property profiles in the boundary layer and free troposphere. Journal of Geophysical Research 97, 12837–12850.

Ross, J.L., Hobbs, P.V., Holben, B., 1998. Radiative characteristics of regional hazes dominated by smoke from biomass burning in Brazil: closure tests and direct radiative forcing. Journal of Geophysical Research 103, 31925–31941.

Sheridan, P.J., Ogren, J.A., 1999. Observations of the vertical and regional variability of aerosol optical properties over central and eastern North America. Journal of Geophysical Research 104, 16793–16805.

Stelson, A.W., 1990. Urban aerosol refractive index prediction by partial molar refraction approach. Environmental Science and Technology 24, 1676–1679.

Tang, I.N., 1996. Chemical and size effects of hygroscopic aerosols on light scattering coefficients. Journal of Geophysical Research 101, 19245–19250.

Watson, J.G., Chow, J.C., Lowenthal, D.H., Cahill, C.F., Blumenthal, D.L., Richards, L.W., 2001. Aerosol chemical properties during the Mt. Zirkel visibility study. Journal of Environmental Quality 30, 1118–1125.

Watson, J.G., 2002. Visibility: science and regulation. Journal of the Air and Waste Management Association 52, 628–713.

Wolff, G.T., 1984. Particulate elemental carbon in the atmosphere. Journal of the Air Pollution Control Association 31, 935–938.